

The Raspberry Model for Hydrodynamic Interactions Revisited, Part I: Periodic Arrays of Spheres and Dumbbells

Lukas P. Fischer,¹ Toni Peter,¹ Christian Holm,¹ and Joost de Graaf^{1,*}

¹*Institute for Computational Physics (ICP), University of Stuttgart, Allmandring 3, 70569 Stuttgart, Germany*

(Dated: July 21, 2022)

The so-called ‘raspberry’ model refers to the hybrid lattice-Boltzmann and Langevin molecular dynamics scheme for simulating the dynamics of suspensions of colloidal particles, originally developed by [V. Lobaskin and B. Dünweg, *New J. Phys.* **6**, 54 (2004)], wherein discrete surface points are used to achieve fluid-particle coupling. This technique has been used in many simulation studies on the behavior of colloids. However, there are fundamental questions with regards to the use of this model. In this paper, we examine the accuracy with which the raspberry method is able to reproduce hydrodynamic interactions in simple-cubic crystals. To this end, we compare our LB simulation results to established theoretical expressions. We show that there is a discrepancy between the translational and rotational diffusion constant reproduced by the simple raspberry model and present a way to remedy the problem by adding internal coupling points. We find that both the original and improved version of the raspberry model reproduce hydrodynamic interactions to a surprising degree of accuracy. However, only the one with internal coupling yields consistency between the effective hydrodynamic radii. Finally, we examine a non-convex shape, namely a colloidal dumbbell, and show that the raspberry model reproduces the desired hydrodynamic behavior in bulk for this more complicated shape. Our investigation is continued in [J. de Graaf, *et al.*, **XX XX**, xx (2015)], wherein we consider the raspberry model in confining geometry of two parallel plates.

I. INTRODUCTION

The physical description of hydrodynamic interactions in fluids has been a field of intensive study for over three centuries. The first mathematical description of (rarefied) flow dates back to Euler. [1] This description was subsequently refined by, a.o., Navier and Stokes to be applicable to the flow of dense media. [2, 3] However, finding solutions to the Navier-Stokes equations, even under the simplifying assumption of the low Reynolds number regime, has proven to be a particularly challenging boundary-value problem. Only in a few simple geometries can the Navier-Stokes equations be analytically solved, often leading to truncated series expansions rather than a full solution.

Two geometries that can be handled semi-analytically are a simple-cubic array of spheres and a sphere between two parallel plates. The former is of particular interest as a toy model for fluid flow in a porous medium (at small sphere separations), [4] while the latter is relevant to, for example, the field of hydrodynamic chromatography. [5, 6] In this paper, we consider the crystalline arrangement and in Ref. [7] we study the confining geometry of two parallel plates.

For the translational movement of a simple-cubic crystal through a fluid, the first results were obtained by Hasimoto, who derived a semi-numerical result for dilute packings. [8] A complete numerical study for a range of lattice spacings and various crystal structures was later presented by Zick and Homsy. [9] The hydrodynamic

flow around an infinite (simple-cubic) array of rotating spheres was first described by Brenner *et al.* [10] These results were subsequently refined by Zuzovsky *et al.* [11] A complete numerical study of both translational and rotational friction over a large range of possible lattice spacings was provided by Hofman *et al.* [4] This large number of semi-analytic investigations makes the simple-cubic geometry perfectly suited for benchmarking the quality of hydrodynamic solvers.

A breakthrough in the numerical simulation of fluid dynamics resulted from the development of the lattice-Boltzmann (LB) algorithm, which is based on the discretized version of the Boltzmann transport equation, see Ref. [12] for a brief background. This lattice-based algorithm allows for the efficient simulation of hydrodynamic interactions in arbitrary geometries using simple boundary conditions, such as the bounce-back rule to obtain no-slip surfaces. [12]

In the early days of LB, moving (bounce-back) boundaries proved difficult to implement. One attempt to tackle this problem was introduced by Ahlrichs and Dünweg, who simulated polymer chains by utilizing an interpolated point-coupling scheme. [13] These points (particles) coupled to the fluid through a frictional force, acting both on the solvent and on the solute, which depends on the relative velocity. The effect of this coupling is the formation of a hydrodynamic hull around the points, which thus behave as particles with a finite hydrodynamic extent (effective hydrodynamic radius). [13] Even if individual friction coefficients are used for the particles, this method is limited in the particle size-ratios that it can handle, namely, by the particle-grid interpolation scheme and discretization used for the LB fluid. [13] Thus it cannot be used to study, *e.g.*, the electrophoresis

* jgraaf@icp.uni-stuttgart.de

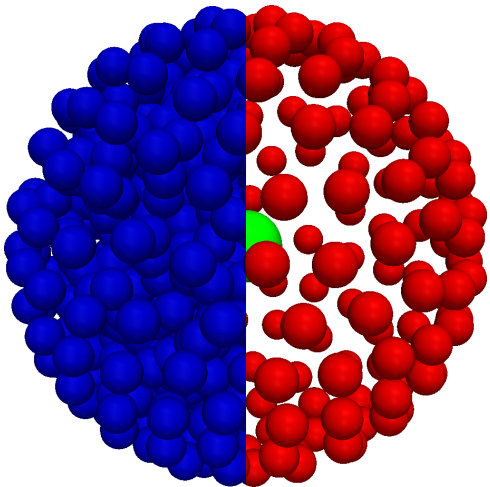


FIG. 1. (color online) Representation of the structure of the raspberry models used in our simulations, filled (left) and hollow (right), respectively. The central bead to which all other beads are connected *via* rigid bonds is shown using a green sphere. The blue spheres represent the beads that form the filled raspberry and the red ones give the surface beads used for the hollow variant. The radius of the beads is chosen to be smaller than the typical effective hydrodynamic radius to help visualize the internal structure.

of colloids with explicit ions.

Lobaskin and Dünweg remedied this issue by introducing the so-called ‘raspberry’ model, in which a larger colloid could be incorporated into the LB algorithm by discretizing the surface into point particles and utilizing the aforementioned coupling scheme. [14] The method derives its name from this discretized nature of the surface, which resembles a raspberry, when represented by molecular-dynamics (MD) beads, see Fig. 1. The raspberry model relies on a proper coverage of the surface by coupling points, such that the fluid inside of the shell is ‘trapped’ and thus moves and rotates in unison with the shell. This creates an effective no-slip/co-moving boundary condition at the surface.

Moving bounce-back (as well as other varieties of) boundary conditions were developed to exploit the lattice structure of the LB in describing colloidal particles. [15, 16] However, the raspberry method has remained popular, because of its simplicity as a straightforward extension of point-particle coupling. It has been extended upon [17, 18] and has been used in a wide variety of simulation settings. [19–21] Recently, this model was employed in the context of multi-particle collision dynamics (MPCD), [22, 23] stochastic rotation dynamics (SRD), [24] and dissipative particle dynamics (DPD) simulations. [25, 26]

From the work of Ollila *et al.* [18] it has become apparent that there are problems with the fluid coupling scheme inherent to the raspberry model. In particular, Ollila *et al.* showed that the hydrodynamic radius

of these particles is ill-defined in an LB fluid. That is, the effective hydrodynamic radius that follows from the translational diffusion coefficient (*via* the Stokes-Einstein relation) does not match that obtained using the rotational diffusion coefficient. Ollila *et al.* also noticed that the kinetic temperature of the particle, measured *via* the equipartition theorem and the temperature of the fluid may differ significantly. By carefully tailoring the coupling, they succeeded in matching the rotational and translational effective radii, as well as the kinetic and fluid temperature.

In this manuscript, we re-examine the raspberry model by Lobaskin and Dünweg [14] in the context of the work of Ollila *et al.* [18] We show that there is a simpler way to obtain a consistent hydrodynamic description using the raspberry model, namely by introducing coupling points to the interior of the raspberry particle. To accomplish this, we examine the quality of the raspberry model in the classic fluid-dynamics geometry of a simple-cubic arrangement. We show that the raspberry model behaves surprisingly well for small separation between the individual raspberries. Finally, we consider the effectiveness of the raspberry description for non-convex particles and show that the model gives accurate results for the bulk diffusion coefficient of a dumbbell-shaped colloid. Part II of our analysis, which extends these conclusions to raspberry particles under confinement, is presented in Ref. [7].

The remainder of this manuscript is structured as follows. In Section II we describe our simulation methods in detail. Section II A introduces our variant of the raspberry model for the spherical and dumbbell-shaped colloids of interest. Sections II B and II C detail the molecular dynamics and LB simulation parameters, respectively. Section II D describes the various hydrodynamic experiments that we performed to determine the properties of the raspberry model. We provide a summary of the notations used throughout the text in Section II E to aid the reader when going through the manuscript. In Section III we list our main results. We begin by examining the properties of the spherical raspberry in a simple-cubic lattice in Section III A. We continue with the properties of two dumbbell-shaped raspberries in Section III B. The results are discussed and related to previous studies in Section IV. Finally, we give a summary, conclusions, and an outlook in Section V.

II. METHODS

In this section, we outline the modeling approaches used to determine the hydrodynamic properties of a colloid. We have split this into subsections detailing the properties and construction of the raspberry model, the molecular dynamics and lattice-Boltzmann parameters used, the hydrodynamic experiments performed to extract the diffusion properties of the raspberry, and a reference list of the input parameters and measured quantities.

A. The Raspberry Model

In this manuscript we study the so-called ‘raspberry’ model for particle-fluid interactions, which was introduced by Lobaskin and Dünweg. [14] The solvent is modeled *via* the lattice-Boltzmann (LB) method and molecular dynamics (MD) is used for the colloid. The coupling between solvent and particles is accomplished using a frictional force acting both on the solvent and on the colloid, which depends on the relative velocity, and acts at discrete points (MD beads) distributed over the particle’s surface.

The MD beads (point particles) that cover the surface gain an effective hydrodynamic radius through their interaction with the fluid, [13] giving the colloid the appearance of a raspberry, which is where the method derives its name from, as seen in Fig. 1. In addition, the fluid coupling with the MD beads forces the fluid inside the particle to move along and co-rotate with the shell, thus making it possible to model a solid object with no-slip/co-moving boundary conditions for sufficiently high fluid-bead friction.

In Ref. [14], 100 points were used to approximate a sphere. To ensure a reasonably homogeneous surface coverage these were connected to each other by finite extensible nonlinear elastic (FENE) potentials. The forces acting on the surface beads were forwarded to a central Lennard-Jones (LJ) MD bead, *via* the LJ interaction. A model similar in spirit to the one proposed by Lobaskin and Dünweg was developed by Chatterji and Horbach. [17] In their construction the surface beads were fixed with rigid bonds to the central bead and no FENE potential was employed for the surface-center coupling.

1. The Hollow Raspberry

For the construction of the raspberry model in this paper, we combined the approaches of Refs. [14, 17]. To arrange the MD beads in a spherical shell of radius R , we used a separate MD simulation. We placed $N \gtrsim [4\pi R^2]$ MD beads in a cubic simulation box with edge length L and periodic boundary conditions. The number of MD beads was chosen such that on average there is at least one particle per lattice site for the LB simulation. To force the beads onto a spherical shell we employed a shifted harmonic bond potential around the center of the box (of the future particle) \mathbf{r}_P . This potential has the form

$$V_{\text{harm}}(\mathbf{r}) = \frac{1}{2}K(|\mathbf{r} - \mathbf{r}_P| - R)^2, \quad (1)$$

where \mathbf{r} is a point in space and K is the spring constant. To ensure that the beads do not overlap and to homogenize the surface density, we endowed them with a repulsive Weeks-Chandler-Anderson (WCA) interaction

potential

$$V_{\text{WCA}} = \begin{cases} 4\epsilon \left(\left(\frac{\sigma}{r}\right)^{12} - \left(\frac{\sigma}{r}\right)^6 + \frac{1}{4} \right) & r < 2^{1/6}\sigma \\ 0 & r \geq 2^{1/6}\sigma \end{cases}, \quad (2)$$

where σ is the MD base unit of length and is equal to the bead diameter.

The MD beads were thermalized using a Langevin thermostat with ‘temperature’ 1ϵ and friction coefficient $\Gamma = 1\tau^{-1}$. Here, ϵ is the MD base unit of energy and corresponds to $1k_B T$, where k_B is the Boltzmann constant and T is the temperature, and τ is the MD base unit of time. The MD beads were given mass $1m_0$, with m_0 the MD base unit of mass ($m_0 = \tau^2\epsilon/\sigma^2$). By geometrically increasing the spring constant from $K = 1\epsilon$ to $K = 3,000\epsilon$ the MD beads are forced onto the spherical shell described by the potential in Eq. (1). We increased K by a factor of 1.1 to its final value of $K = 3,000\epsilon$ over 100,000 integration steps of length $\Delta t = 0.003\tau$. These simulations were performed using the MD software package *ESPReso*. [27, 28] Finally, small deviations of the MD beads’ radial position with respect to the desired distance R were removed by adjusting their radial position. The configuration was then ‘frozen in’ by connecting all beads to a central bead via rigid bonds (virtual sites). [28]

To test the quality of the result, the raspberry was checked for large holes in the surface coverage by applying a ‘shotgun’ algorithm. We randomly picked 50,000 points on the surface of the sphere and calculate the distances to the nearest surface bead. We arrived at the distribution of MD beads that we used throughout our simulations, by repeating this procedure with different initial configurations and particle numbers, until we found a system for which the maximum hole size was roughly 1σ (bead diameter). The result for a sphere of radius $R = 3\sigma$ is shown in the right-hand side of Fig. 1. Here, 202 surface beads were used to obtain a maximal hole diameter of 1.1σ . We refer to this model as a ‘hollow raspberry’ for the remainder of this manuscript.

2. Filling the Raspberry

We ‘fill’ the hollow-shell raspberry particle by adding coupling points in the interior, as outlined in detail below. We first formed a hollow raspberry according to the recipe in Section II A 1. Next, we added $N' \gtrsim [4\pi(R - \sigma/2)^3/3]$ beads to the interior of the shell, which interact with each other and the shell MD beads via the WCA potential of Eq. (2). The force between the internal beads themselves was initially capped to $1\epsilon/\sigma$ to prevent numerical instabilities. The system was allowed to evolve by making use of a Langevin thermostat ($k_B T = 1\epsilon$, $\Gamma = 1\tau^{-1}$). Over 50,000 time steps of length $\Delta t = 0.005\tau$ were used during which the capping value was slowly raised to 100ϵ . This generally resulted in a random configuration with a homogeneous distribution of MD beads within the raspberry. These particles

were subsequently frozen in place by adding rigid (virtual) bonds to the central MD bead.

We examined several values of N' and investigated the homogeneity of the distribution of MD beads. We settled upon a value of $N' = 722$, resulting in a total of $N_{\text{tot}} = N + N' + 1 = 925$ MD beads for the so-called ‘filled raspberry’ of radius $R = 3\sigma$. This result is shown in the left-hand side of Fig. 1. Note that we used exactly the same hollow shell to construct our filled variant. Finally, it should be remarked that in the hydrodynamic simulations utilizing the raspberry model, all WCA interactions were switched off and only the rigid (virtual) bonds remained. We only considered a single colloid moving in bulk, which does not collide with itself.

3. Constructing a Dumbbell Raspberry

A dumbbell-shaped raspberry model (filled or hollow) is constructed using a procedure that is analogous to the one given in Sections II A 1 and II A 2. Instead of a central harmonic potential, we used two harmonic potentials centered on $\mathbf{r}_P = (0, 0, -d/2)$ and $\mathbf{r}'_P = (0, 0, d/2)$, with d the distance between the sphere centers of the dumbbell (the length is $d + 2R$). In addition, a WCA potential had to be added to prevent particles from accumulating in the neck of the dumbbell – the region where the two dumbbell spheres overlap, if $d < 2R$. To accomplish this, we used a WCA potential between the center of the dumbbell, located at $(0, 0, 0)$, and the surface MD beads. This potential had the following form

$$V_{\text{neck}} = \begin{cases} 4\epsilon \left(\left(\frac{w}{r}\right)^{12} - \left(\frac{w}{r}\right)^6 + \frac{1}{4} \right) & r < 2^{1/6}w \\ 0 & r \geq 2^{1/6}\sigma \end{cases}, \quad (3)$$

where w is the width of the neck and is given by

$$w = \sqrt{R^2 - \frac{d^2}{4}}. \quad (4)$$

After letting the particles become trapped in the dumbbell shell, in the same manner as for the spherical shell, they are connected *via* rigid bonds to a particle at the center of the dumbbell. The dumbbell may be filled with N' additional beads using the procedure outlined in Section II A 2. In this paper, we consider two dumbbell-shaped raspberry particles – one with $d = 5\sigma$ and one with $d = 7\sigma$ – corresponding to a partially overlapping configuration and one with the spheres just touching, respectively; see Fig. 2. We used $(N = 416, N' = 598)$ for $d = 5\sigma$ and $(N = 502, N' = 404)$ for $d = 7\sigma$, respectively, to ensure a homogeneous surface distribution and filling of the volume.

B. Molecular Dynamics Parameters

Once the raspberries had been constructed, we were able to use them in our LB simulations. The particles

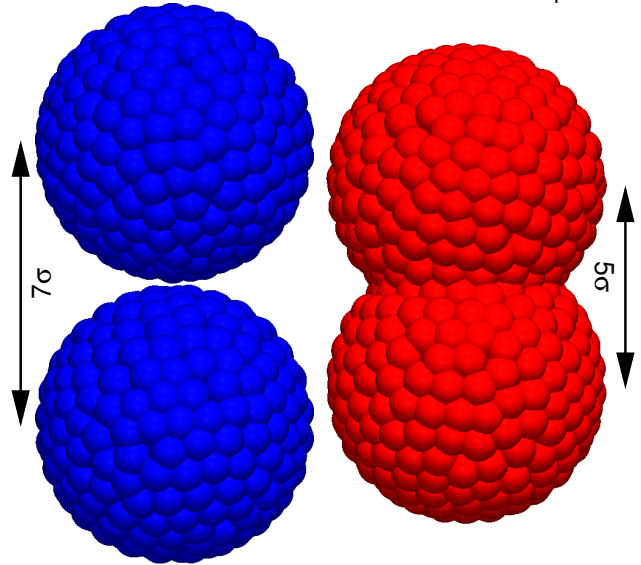


FIG. 2. (color online) Representation of the raspberry dumbbells used in our simulations, touching (left) and overlapping (right), respectively. The distance between the centers of the spheres (each $R = 3\sigma$ in size) is indicated using the arrows. Note that we used the effective MD bead diameter of approximately 1σ to visualize our result.

were allowed to freely move and rotate, unless otherwise specified. All the forces acting on the MD beads are transferred to the central bead *via* the virtual sites (rigid bonds). To stabilize the simulation for the bare friction coefficients used, we set the mass and rotational inertia. These quantities were based on the particle’s dimensions and the fluid mass density, which we denote by ρ and set to $\rho = 1m_0\sigma^{-3}$. For the sphere the mass is $m = (4/3)\pi\rho R^3 \approx 113m_0$ and the inertia tensor is a diagonal tensor with identical entries of $(8/15)\pi\rho R^5 \approx 407m_0\sigma^2$.

In the case of the two dumbbell raspberries we used

$$m = \begin{cases} \pi\rho \left(\frac{4}{3}R^3 + dR^2 - \frac{1}{12}d^3 \right) & 0 \leq d < 2R \\ \frac{8}{3}\pi\rho R^3 & d \geq 2R \end{cases}, \quad (5)$$

for the mass. The rotational inertia tensor is diagonal, but the entries are not identical. Let I_{\parallel} denote the moment for rotation about the main axis of the dumbbell and I_{\perp} the moment for rotation about a central axis perpendicular to the main axis. We may then write

$$I_{\perp} = \begin{cases} \pi\rho \left(\frac{8}{15}R^5 + \frac{3}{4}dR^4 + \frac{1}{3}d^2R^3 + \frac{1}{24}d^3R^2 + \frac{1}{960}d^5 \right) & 0 \leq d < 2R \\ \pi\rho \left(\frac{8}{15}R^5 + \frac{2}{3}d^2R^3 \right) & d \geq 2R \end{cases}; \quad (6)$$

$$I_{\parallel} = \begin{cases} \pi\rho \left(\frac{16}{15}R^5 + \frac{1}{2}dR^4 - \frac{1}{12}d^3R^2 + \frac{1}{160}d^5 \right) & 0 \leq d < 2R \\ \frac{16}{15}\pi\rho R^5 & d \geq 2R \end{cases}; \quad (7)$$

$$\underline{\underline{I}} = \begin{pmatrix} I_{\perp} & 0 & 0 \\ 0 & I_{\perp} & 0 \\ 0 & 0 & I_{\parallel} \end{pmatrix}, \quad (8)$$

where the long axis of the dumbbell is assumed to be aligned with the z -axis. This gives us the following for the $d = 5\sigma$ dumbbell: $m \approx 221m_0$, $I_{\perp} \approx 2226m_0\sigma^2$, and $I_{\parallel} \approx 810m_0\sigma^2$. Whereas for the $d = 7\sigma$ dumbbell we obtain: $m \approx 226m_0$, $I_{\perp} \approx 3585m_0\sigma^2$, and $I_{\parallel} \approx 814m_0\sigma^2$.

C. Lattice-Boltzmann Parameters

The raspberry particles were coupled to a lattice-Boltzmann (LB) fluid. We used a graphics processing unit (GPU) based LB solver, [29] which is attached to the MD software *ESPResSo*. [27, 28] The GPU variant of LB implemented in *ESPResSo* utilizes a D3Q19 lattice and a fluctuating multi-relaxation time (MRT) collision operator. [30] This fluctuating LB model was introduced first by Adhikari *et al.* [31] and later validated by Dünweg *et al.* [32, 33] The particle-fluid interaction proposed by Ahlrichs and Dünweg [13] was used to couple the fluid to embedded MD beads. We did not employ the coupling scheme by Ollila *et al.* [18] The particle coordinates were interpolated onto the lattice using a tri-linear scheme. [12]

To keep our result as general as possible, we set the density of the fluid to $\rho = 1m_0\sigma^{-3}$, the lattice spacing to 1σ , the time step to $\Delta t = 0.005\tau$, the (kinematic) viscosity to $\nu = 1\sigma^2\tau^{-1}$, the bare particle-fluid friction to $\zeta_0 = 25\tau^{-1}$, and the strength of the fluctuations to $k_B T = 0.01\epsilon$, unless otherwise specified. Here, we chose neither to optimize our parameters for the most accurate reproduction of hydrodynamic interactions, nor to match a specific experimental system of interest *via* telescoping. [34, 35] The reason behind our choice is to use parameters that are in the regime, where LB reproduces hydrodynamic effects reasonably well and is sufficiently stable to use the (float-precision) GPU algorithm; thus making our results ‘generic’ rather than tailored to a specific system. The low amplitude of the fluctuations in the thermalized LB is to allow averaging over long times without noise dominating our results, as will become more clear when we discuss these.

D. Hydrodynamic Experiments

To assess the quality of the raspberry approximation in modeling the hydrodynamic properties of a colloid we performed several experiments. We use the term ‘quiescent’ to describe an un-thermalized (non-fluctuating) LB fluid. Below we specify the experiments performed for particles in a simple cubic lattice, *i.e.*, a cubic simulation box of length L with periodic boundary conditions. In all experiments the particle was initialized in the center of the box.

- A *force* experiment in a quiescent fluid, see Fig. 3(a). A constant force \mathbf{F} was applied to the particle (typically along one of the box axes) and a counter force density of $-\mathbf{F}/L^3$ was applied homogeneously to the fluid to ensure that there was no motion of the center of mass. The resulting time-dependent velocity $\mathbf{v}(t)$ and terminal velocity \mathbf{v}_t were measured and used to determine the translational diffusion coefficient *via* the Einstein-Smoluchowski relation

$$D^T = k_B T \mu \equiv k_B T \frac{|\mathbf{v}_t|}{|\mathbf{F}|}, \quad (9)$$

where D^T is the translational diffusion coefficient and μ is the particle’s mobility.

- A *force* experiment in a thermalized fluid, see Fig. 3(b). The set-up is the same as for the first experiment. However, the system was first equilibrated until a steady-state had emerged and the particle fluctuated with the proper thermal distribution. During the production run, $\mathbf{v}(t)$ was averaged to determine the average terminal velocity $\bar{\mathbf{v}}_t = \langle \mathbf{v}(t) \rangle$, where $\langle \cdot \rangle$ denotes the time average.
- A *torque* experiment in a quiescent fluid, see Fig. 3(c). A constant torque \mathbf{T} was applied to the particle (typically along one of the box axes). The resulting time-dependent angular velocity $\boldsymbol{\omega}(t)$ and terminal angular velocity $\boldsymbol{\omega}_t$ were measured and

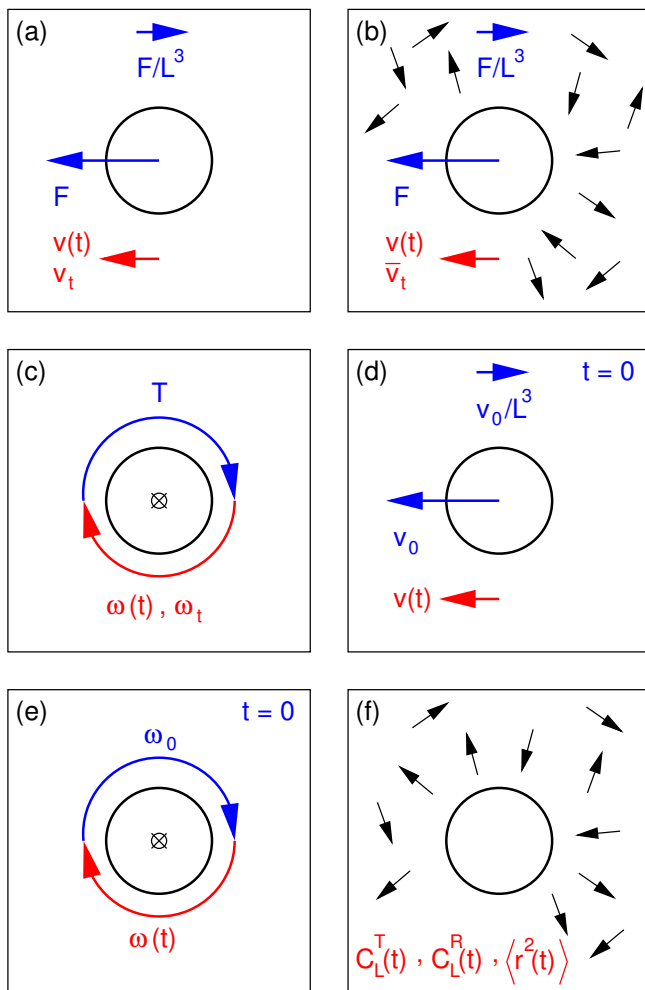


FIG. 3. (color online) Visualization of the various hydrodynamic experiments carried out in a cubic box of length L with periodic boundary conditions. A two-dimensional (2D) representation is given here. The blue arrows and symbols denote quantities applied to the fluid and raspberry, the red arrows and symbols indicate measured quantities. The black arrows indicate a thermalized fluid. We refer to the text for a description of the experiments, as well as the applied and measured quantities.

used to determine the rotational diffusion coefficient *via* the rotational Einstein-Smoluchowski relation

$$D^R = k_B T \frac{|\omega_t|}{|\mathbf{T}|}, \quad (10)$$

where D^R is the rotational diffusion coefficient.

- A *velocity* experiment in a quiescent fluid, see Fig. 3(d). An instantaneous velocity \mathbf{v}_0 was imparted on the particle at $t = 0$ and an instantaneous counter velocity of $-\mathbf{v}_0/L^3$ was applied homogeneously (at the same time) to the fluid to ensure zero motion of the center of mass. The re-

sulting time-dependent velocity $\mathbf{v}(t)$ was measured. This quantity can be related to the velocity auto-correlation function (VACF) $C^T(t)$ *via*

$$C^T(t) \equiv \langle \mathbf{v}(t') \cdot \mathbf{v}(t' + t) \rangle = \frac{3k_B T}{m|\mathbf{v}_0|^2} \mathbf{v}_0 \cdot \mathbf{v}(t), \quad (11)$$

where \cdot denotes the dot product.

- An *angular velocity* experiment in a quiescent fluid, see Fig. 3(e). A instantaneous angular velocity ω_0 was imparted on the particle at $t = 0$. The resulting time-dependent angular velocity $\omega(t)$ was measured. This quantity can be related to the angular velocity auto-correlation function (AVACF) $C^R(t)$ *via*

$$C^R(t) \equiv \langle \omega(t') \cdot \omega(t' + t) \rangle = \frac{3k_B T}{m|\omega_0|^2} \omega_0 \cdot \omega(t). \quad (12)$$

The aforementioned VACF and the above AVACF can be used to compute the translational and rotational diffusion coefficient, respectively, *via* the Green-Kubo relation

$$D^X = \frac{1}{3} \int_0^\infty C^X(t) dt, \quad (13)$$

where the factor $1/3$ is used for spherical particles only and X can be either T or R . The relations for anisotropic particles are similar, but slightly more involved, since the dot product for the (A)VACF is replaced by the dyadic product.

- An *auto-correlation* experiment in a thermalized fluid, see Fig. 3(f). The system was equilibrated until the particle fluctuated with the proper thermal distribution. The (A)VACF and the mean square displacement (MSD) were measured using the multiple-tau correlator in *ESPReso*. [36] For the (A)VACF the (angular) velocity in the co-rotating frame was averaged.

In the above experiments, care was taken to ensure that the particle remained in the low translational Reynolds number regime

$$Re^T = \frac{vR}{\nu} \ll 1, \quad (14)$$

with v the maximum/typical velocity. This implies that we can compare it to analytic and numerical results obtained by solving the Stokes equations, as will be discussed further in Section III. For the radius $R = 3\sigma$ colloid and our value of the kinematic viscosity, we ensured that the maximum particle velocity remained under $0.15\sigma\tau^{-1}$, for which $Re^T < 0.5$. However, this value

was only attained in the *velocity* and *auto-correlation* experiments in the cubic geometry at the initial time. For $t \gg 1\tau$ and in the other experiments, the Reynolds number remained smaller than 0.1. Similarly the rotational Reynolds number

$$Re^R = \frac{\omega R^2}{\nu}, \quad (15)$$

with ω the maximum angular velocity, remained small: $Re^R < 0.7$ throughout, but typically smaller than 0.1.

E. Notations Used throughout this Manuscript

In this section, we summarize the notations used throughout this manuscript. This will aid in the understanding of our results, as many of the notations are necessarily similar.

- L , the box length of a cubic box with periodic boundary conditions.
- R_h^T , the effective hydrodynamic radius obtained by extrapolating translational diffusion measurements, see Figs. 3(a,b,d,f), for the limit of box length $L \uparrow \infty$. The subscript h is used to differentiate R_h from the raspberry radius R .
- R_h^R , the effective hydrodynamic radius obtained by extrapolating rotational diffusion measurements, see Figs. 3(c,e,f), for the limit of box length $L \uparrow \infty$.
- $C_L^T(t)$, the velocity auto-correlation function (VACF) for translational movement in a cubic box of length L with periodic boundary conditions, also see Figs. 3(d,f).
- $C_L^R(t)$, the angular velocity auto-correlation function (AVACF) for rotation in a cubic box of length L with periodic boundary conditions, also see Figs. 3(e,f).
- D_0^T , the bulk translational diffusion coefficient.
- D_0^R , the bulk rotational diffusion coefficient.
- $D_L^T(t)$, the time-dependent translational diffusion coefficient in a cubic box of length L with periodic boundary conditions, also see Fig. 3(a).
- $D_L^R(t)$, the time-dependent rotational diffusion coefficient in a cubic box of length L with periodic boundary conditions, also see Fig. 3(c).
- f , the fractional deviation between two results when reading the text.

Please refer to Fig. 3 and the above list if there is any confusion.

III. RESULTS

In this section, we discuss the results that we obtained by performing the simulations and numerical calculations

outlined in Section II. We have split these into two parts: one for the sphere and one for the dumbbell. These parts are further subdivided according to the nature of the experiments.

A. Sphere in a Simple Cubic Crystal

1. Comparison of the Velocity Auto-Correlation Functions

Using the (quiescent) *velocity* and (thermalized) *auto-correlation* experiments discussed in Section IID, see Figs. 3(d,f), we established the VACF for a filled raspberry sphere in a cubic box of length $L = 100\sigma$. The result is shown in Fig. 4. From Figs. 4(a,b,c) we observe the three (possibly four) decay regimes that are typical for the LB simulations of the raspberry particle.

(I) At short times there is an unphysical-coupling regime, see Fig. 4(a), in which the VACF decays exponentially according to

$$C_L^T(t) \propto \exp\left(-\frac{N_{\text{tot}}\zeta_0}{m}t\right), \quad (16)$$

with N_{tot} the total number of beads, ζ_0 the bare friction coefficient, and m the particle's mass. The existence of this regime can be attributed to the fluid not moving along with the velocity of the particles. That is, the MD beads interact with the stationary fluid only through a regular Langevin-type friction – the velocity of the fluid is essentially zero in these time steps. This implies that the no-slip boundary condition at the surface of the raspberry is violated; a problem inherent to the coupling method. [14, 17]

The expected (unphysical) decay of Eq. (16) is indicated in Fig. 4(a) and corresponds reasonably well with the observed initial decay. However, the result deviates even in the first and second time step, signifying the onset of proper coupling. This is in agreement with the recent observations in the MPCD simulations of Ref. [23], where this deviation from the expected unphysical decay was also attributed to the onset of hydrodynamic correlations. Finally, note that there is a small deviation between the thermalized LB result and the quiescent VACF when $t > 0.03\tau$, to which we will come back later.

(II) At intermediate times there is a regime, in which the VACF decays exponentially according to Stokes' prediction

$$C_L^T(t) \propto \exp\left(-\frac{6\pi\eta R}{m}t\right). \quad (17)$$

This regime appears because the hydrodynamic coupling between the particles and the surrounding is now fully established. [14, 17] The match between Stokes' prediction and our numerical results can be appreciated in Fig. 4(b), where a Stokes-type decay has been fitted to our data. The agreement is reasonable over a regime of about one

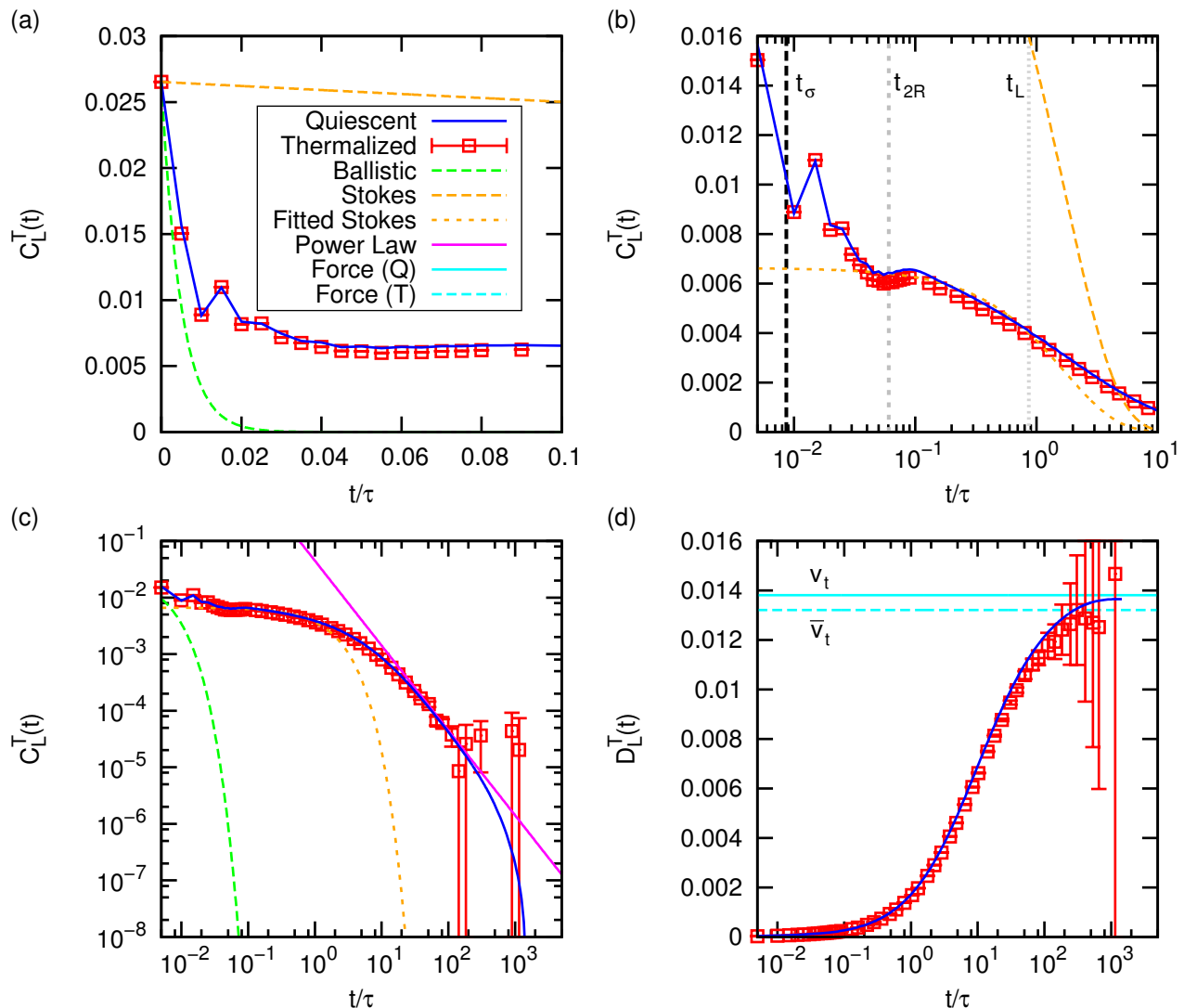


FIG. 4. (color online) The velocity auto-correlation function (VACF) $C_L^T(t)$ as a function of time t expressed in the MD time unit τ . The graphs show results for a filled raspberry of radius $R = 3\sigma$ in a box of length $L = 100\sigma$, with LB parameters as given in the text. (a) The initial decay of the VACF. The red squares with error bars show the result for a thermalized LB, while the blue solid curve gives the result for a quiescent experiment, scaled to start with the thermal velocity, see Eq. (11). The dashed orange curve shows Stokes' solution for the initial decay and the green dashed line the unphysical-coupling decay inherent to LB. (b) Log-linear plot of the initial and intermediate decay of the VACF. The orange curve with short dashes gives Stokes' decay, which has been fitted to the exponential decay that follows the unphysical-coupling regime. For completeness, the unfitted Stokes' solution is also shown. The vertical lines indicate the time for sound waves to propagate through the system over certain lengths: one lattice spacing (t_σ , dashed black), roughly the inter-bead separation; the raspberry's hydrodynamic diameter (t_{2R} , dashed gray); and the box length (t_L , dotted gray). (c) Log-log plot of the long-time decay. The magenta line is a fit to the power-law decay ($t^{-3/2}$) that sets in after the initial sound waves have traveled the length of the box. The unphysical-coupling and fitted Stokes' curves are shown for completeness. (d) The time-dependent Green-Kubo value of the translational diffusion constant $D_L^T(t)$ from the quiescent (blue solid curve) and thermalized (red squares with error bars) LB result. The solid cyan line shows the result of a quiescent force experiment (derived from the terminal velocity v_t), while the dashed cyan line shows the result of a thermal-averaged force experiment (from the time-averaged terminal velocity \bar{v}_t).

decade. Had the LB algorithm satisfied the Stokes' solution instantaneously, the onset of a Stokesian exponential decay would have been immediate. The result of instantaneous fulfillment of Stokes' decay is shown in Fig. 4(a) and the deviation between the LB result and the predic-

tion is considerable.

We have indicated a total of three times related to sound propagation in the LB in Fig. 4(b). The speed of

sound in LB is given by

$$v_s = \sqrt{\frac{1}{3}} \left(\frac{\sigma}{\Delta t} \right), \quad (18)$$

where σ is the lattice spacing, $\Delta\tau$ is the time step, and the prefactor stems from the dimensionality of the grid. The three times are $t_\sigma = \sigma/v_s$, $t_{2R} = 2R/v_s$, and $t_L = L/v_s$, *i.e.*, the time required for sound waves to propagate one lattice spacing, the diameter of the raspberry, and the length of the box, respectively. We will now discuss the relevance of these times.

For the filled sphere, in which the MD beads are roughly 1σ apart, we find possible signatures of the propagation of sound between the MD beads, as can be inferred from the short-time oscillations. The first dip in the VACF roughly coincides with t_σ , as indicated by the black dashed line in Fig. 4(b). These oscillations may also be related to the magnitude of the effective friction that the added coupling points in the interior bring about. At the time it takes sound to propagate the diameter of the sphere (t_{2R}), we find a small dip in the VACF, see the dashed gray line in Fig. 4(b). This dip is similar to the one observed in Ref. [23] and is caused by the compressibility of the LB fluid. Note that the Stokesian regime of decay appears to be delimited by the time it takes sound to travel the distance of the box (t_L , dotted gray line in Fig. 4(b)). However, for our specific choice of parameters, this time is close to the viscous time it takes momentum to diffuse by one colloidal radius $t_\eta = \rho R^2/\eta = 9\tau$. This viscous time is the relevant time scale for the development of hydrodynamic memory effects. We have a stricter separation of sonic and viscous time scales than in Refs. [22, 23], *i.e.*, $t_\eta/t_{2R} \gg 1$. Therefore, our results do not display sound undulations (back tracking) in the long-time power-law regime.

(III) After a sufficiently long time, the hydrodynamic interactions with the surrounding fluid result in a persistence of the velocity (non-exponential decay) as the vorticity diffuses away from the particle. These hydrodynamic memory effects lead to an algebraic decay of the VACF; the so-called ‘long-time tail’. [37] This decay has the following form

$$C_L^T(t) \propto t^{-3/2}, \quad (19)$$

where the value of the exponent is related to the translational motion. Figure 4(c) shows this power-law decay more clearly by means of a fit. Note that within the error bar, which gives the standard error, the decay is captured by the thermalized result. The data is not very convincing, but it was the best that could be achieved within a reasonable time frame for our choice of parameters. Only for $L \gg 1\sigma$ is the regime over which there is power-law decay more pronounced, however, larger box sizes require even longer sampling. Our result is similar to the ones observed in Refs. [14, 17].

(IV) For the quiescent data, there is a third exponential decay in the data when $t \gg \tau$, see the blue line in

Fig. 4(c). Analysis shows that this decay has a similar exponent as the unphysical-coupling decay that occurs at short times. The exponential decay for $t \gg \tau$ is most likely a numerical artifact, due to the low velocity of both the particle and the liquid. It is conceivable that the velocity of the fluid decays faster than that of the particle, therefore causing the unphysical-coupling regime to set in again. This regime is not relevant to the physics of the particle, though, since the decay to zero fluid velocity occurs only for the quiescent fluid. For the thermal data it is not possible to judge whether such a regime sets in, since the error bar is too large. However, since the thermalized LB fluid has a far greater local flow profile than the quiescent result (for long times), it is likely that such a regime is absent.

Finally, we considered the Green-Kubo relation for the VACF by taking the anti-derivative

$$D_L^T(t) = \frac{1}{3} \int_0^t C_L^T(t') dt', \quad (20)$$

This gives us the time-dependent translational diffusion coefficient $D_L^T(t)$ shown in Fig. 4(d). We obtained the value of $D_L^T \equiv D_L^T(t \uparrow \infty) = 1.37 \cdot 10^{-2} \sigma^2 \tau^{-1}$ from the quiescent data for the box of length $L = 100\sigma$. The data for the thermalized LB lies slightly lower than the quiescent result, which can in part be attributed to the deviation that was already present at short times. In addition to determining D_L^T from the VACFs we performed a quiescent and thermalized force experiment. The result is shown using the solid and dashed cyan lines in Fig. 4(d), respectively. We arrived at $D_L^T = 1.38 \cdot 10^{-2} \sigma^2 \tau^{-1}$ for the quiescent data and $D_L^T = 1.32 \cdot 10^{-2} \sigma^2 \tau^{-1}$ for the thermalized data. The results from the VACF and the force experiments correspond within the error, but there is a discrepancy between the thermal and quiescent data. This deviation can be explained by the way these experiments are carried out, as will become clear when we discuss the effect of box size in Section III A 2.

In order to examine the difference between the hollow and filled raspberry model, we carried out similar experiments for a hollow-raspberry sphere in a box of length $L = 80\sigma$. The resulting auto-correlation functions are shown in Fig. 5. For the VACF, see Fig. 5(a), the various decays are in qualitative agreement. However, there is weaker coupling between the hollow raspberry and the fluid. This is caused by the spatial distribution of coupling points, not the amount of points, as we will see in Section III A 2. This ‘hollow’ distribution results in weaker decay of the unphysical-coupling regime, which therefore matches the exponential form of Eq. (16) more closely. N.B. This is not a desirable quality. For the AVACF, see Fig. 5(b), we find similar trends. The exponent of the power-law decay for the rotational diffusion coefficient is $5/2$ rather than $3/2$. Note that the existence of this a power-law behavior is more convincingly shown by our AVACF data, as the fitted function and measured decay correspond well over a decade in time.

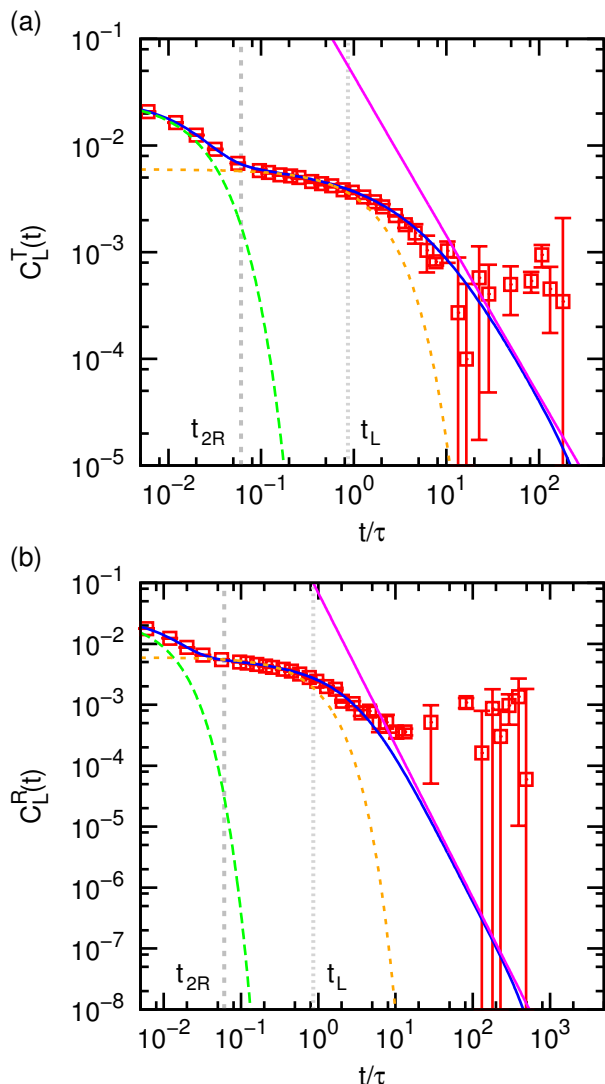


FIG. 5. (color online) Auto-correlation functions for a hollow raspberry of radius $R = 3\sigma$ in a box of length $L = 80\sigma$ as a function of time t expressed in the MD time unit τ . The LB parameters are as given in the text. The use of symbols is the same as in Fig. 4. (a) Velocity auto-correlation function (VACF) $C_L^T(t)$ for the thermal (red squares with error bars) and quiescent (blue curve) calculations. The unphysical-coupling (dashed green), fitted Stokes (dashed orange), and power-law decay (magenta) are also shown. The two dashed vertical lines show the time it takes for sound to travel the particle’s hydrodynamic diameter (t_{2R} , dashed) and the box length (t_L , dotted), respectively. (b) The angular-velocity auto-correlation function (AVACF) $C_L^R(t)$ for the same parameters. The fitted power law-decay scales with $t^{-5/2}$ in this case.

2. The Influence of Lattice Spacing

Thus far, we have examined only the results of the (angular) velocity experiments, and shown that these correspond – at least internally – to the results of force ex-

periments for the same system. Let us now consider the effect of the lattice spacing on the hydrodynamic coupling between the spheres in our effective simple cubic crystal. This simple cubic geometry is unlike a physical crystal, in the sense that all particles translate and rotate in unison – an effect of there being only a single particle in a box with periodic boundary conditions. There is experimental evidence that such systems may be achieved, [38–40] but these can be considered atypical systems. However, this uniform quality makes the solutions to Stokes’ equations for this geometry analytically tractable. Such calculations were performed, for example, in the work of Hasimoto [8] and of Hofman *et al.* [4]. When the raspberry model shows proper behavior in the reduced geometry of the uniform simple-cubic lattice, it can be inferred that the results for more complicated spatial configurations will be reasonable as well.

Figure 6(a) shows the change in velocity $v(t)$ during a force experiment, see Fig. 3(a), for a number of box sizes L using the filled raspberry model. Note that for larger L the friction experienced by the particle is smaller, as the hydrodynamic-interaction contribution of periodic images is reduced. However, the time it takes for the stationary state to set in is increased, as it takes longer to transfer momentum between the particle and its images. From the terminal velocities in the stationary state we determined the diffusion coefficient *via* the Einstein-Smoluchowski relation.

In order to establish the diffusion coefficient at infinite dilution (one particle in a fluid of infinite extent), we fitted our data using a polynomial of the Hasimoto form $a + b/L + c/L^3$ [8] and extrapolated to $L \uparrow \infty$. The resulting value for a is the bulk translational diffusion coefficient D_0^T . From the Stokes-Einstein relation it follows that

$$D_0^T = \frac{k_B T}{6\pi\eta R_h^T} \quad (21)$$

with R_h^T the translational hydrodynamic radius. We were able to determine the effective hydrodynamic radius of our raspberry colloid, using Eq. (21) and the extrapolated value D_0^T . These two parameters D_0^T and R_h^T allowed us to de-dimensionalize the box length and the measured translational diffusion coefficient, as shown in Fig. 6b.

In Figs. 6(b,c) we compare the quality of our result for the box-size dependence with the analytic result by Hasimoto [8] (dashed red curve) and the numerical calculations by Hofman *et al.* [4] (dashed green curve). Figure 6(c) shows the fractional deviation f of our data to the two literature results, as well as the difference between the Hasimoto (Ha) and Hofman *et al.* (Ho) data. For the data points provided by Hofman *et al.* [4] we used a polynomial fit of the form $1 + a/L + b/L^3$ to represent these as a curve. Note that the analytic and numerical expressions of Refs. [4, 8] correspond well for box sizes greater than $L \approx 5.0R_h^T$. That is, within the error that can be expected for the fitting procedure that we applied to the data by Hofman *et al.*, there is good agreement

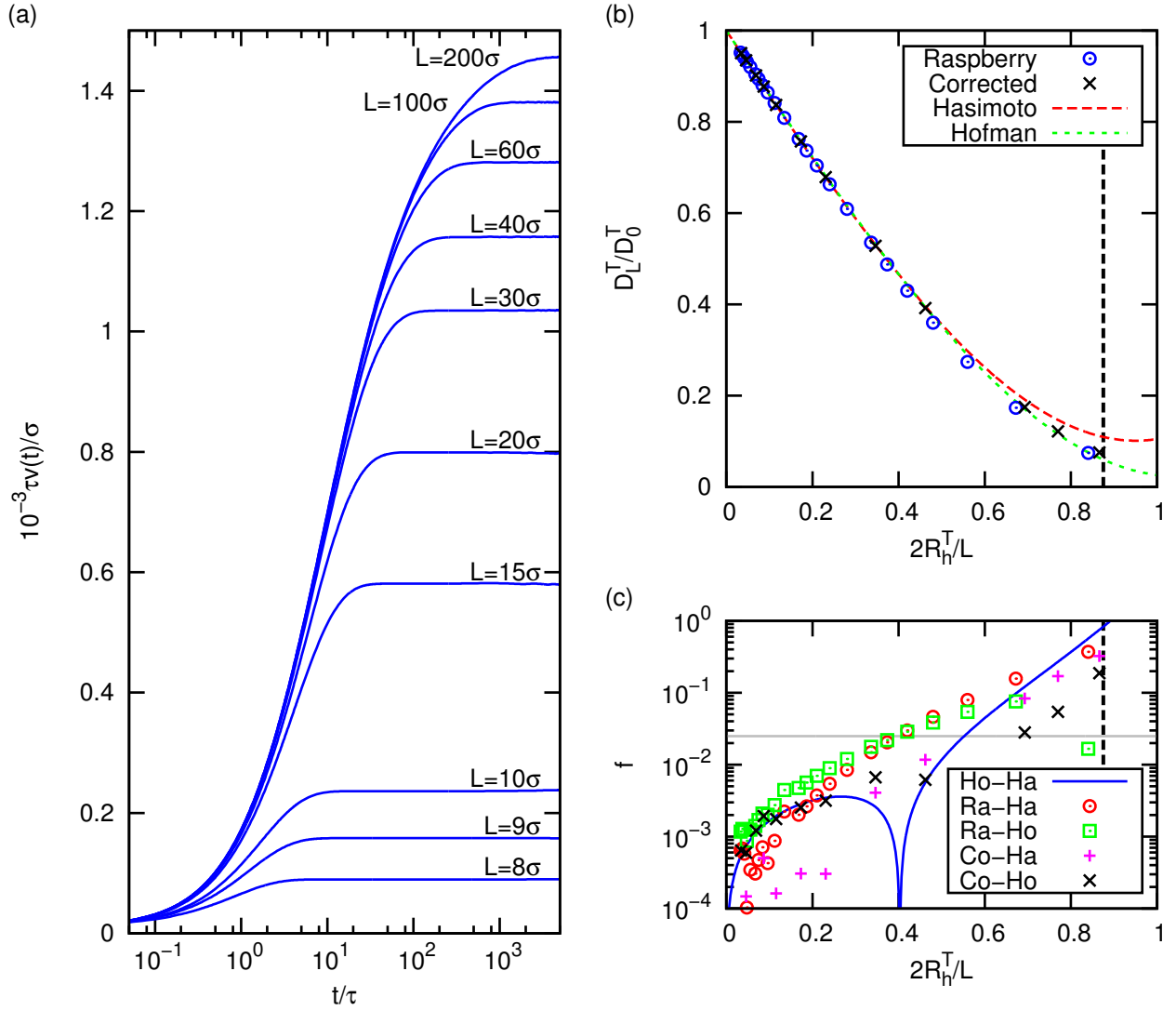


FIG. 6. (color online) (a) The velocity $v(t)$ as a function of time t expressed in the MD time unit τ obtained from force experiments for a selection of box sizes L . (b) The dependence of the particle's translational diffusion coefficient D_L^T (expressed in terms of the bulk translational diffusion coefficient D_0^T) on the inverse box length $1/L$ times the hydrodynamic diameter (twice the hydrodynamic radius R_h^T). The blue circles show results obtained from the velocity experiment. The black crosses give the results of the force experiment, corrected for the counter force applied inside of the raspberry, as explained in detail in the main text. The red dashed curve shows the analytic expression by Hasimoto [8] and the green dashed curve shows a fit to the numerical data of Hofman *et al.* [4]. The vertical dashed line indicates the value of L for which the spheres are separated by one lattice spacing ($L = 2R_h^T + \sigma$). (c) Fractional deviation f as a function of $2R_h^T/L$. The solid blue curve shows the difference between the theoretical expressions of Hasimoto and Hofman. The red circles and green squares indicate the difference between our raspberry experiment and the Hasimoto and Hofman expressions, respectively. The magenta pluses and black crosses give the difference between the force-corrected data and the Hasimoto and Hofman expressions, respectively. The gray horizontal line indicates a fractional deviation of 2.5%.

between their and Hasimoto's data in this regime. The discrepancy for smaller box sizes can be explained by the truncation of the series expansion that was used in Hasimoto's work.

Our raspberry results (Ra) agree reasonably well with the data of Hofman *et al.* over the range $L \gtrsim 5.0R_h^T$, but there is also a clear signature of systematic deviation present in f . This implies that our data differs substan-

tially from the values of Ref. [4] in the $1/L^3$ term. A similar range of agreement and small-box-size deviation can be observed between our data and that of Hasimoto. However, in spite of this, our data is much closer to the results of Hofman *et al.* than those of Hasimoto; by almost an order of magnitude in f for $L \downarrow 2R_h^T$. We will discuss the origin of the systematic deviation between our data and that of Ref. [4] next.

The discrepancy between our data and the result by Hofman *et al.* brings us back to the difference that we observed between the VACFs obtained from the velocity and temperature experiments carried out in Section III A 1. Remember that in the quiescent experiments a homogeneous and instantaneous velocity has to be applied to the fluid in order to ensure zero movement of the center of mass, see Fig. 3(d). Similarly, for the quiescent force experiment, a constant homogeneous force density is applied to the fluid, see Fig. 3(a). This has the consequence that this velocity and force are also applied directly to fluid nodes that are coupled to raspberry MD beads. The effective force applied to the colloid is therefore

$$\mathbf{f}_{\text{eff}} = \mathbf{f} \left(1 - \frac{4\pi R^3}{3L^3} \right). \quad (22)$$

Analogously, the counter velocity may affect the time evolution of the VACF. For the thermalized experiments this was not an issue, since counter velocities and forces do not need to be applied. These counter velocities and forces are therefore a likely candidate for the observed discrepancies.

We used the effective force of Eq. (22) to determine the ‘corrected’ value of $D_L^T(\text{Co})$ via the Einstein-Smoluchowski relation (Eq. (9)) as a function of the box size, see Fig. 6(b). Note that the correspondence between the result by Hofman *et al.* and our data is thus greatly improved and that the systematic deviation is removed for large box sizes. Moreover, for small box sizes the deviation between our corrected result and the literature values is substantially reduced, although a systematic signature remains. Within the error the data corresponds much closer to the curve given by Hofman *et al.* than it does to the Hasimoto result.

From our corrected data, we estimated the range over which the raspberry is able to accurately reproduce hydrodynamics interactions ($f < 2.5\%$) in our system. For this particular model we found the criterion to be $L \gtrsim 2.8R_h^T$, which, as mentioned before, could be extrapolated to other spatial arrangements of the colloids. The results for a hollow raspberry lie on top of the filled ones shown in Fig. 6(b) within the error bar. However, the values for the effective hydrodynamic radii R_h^T differ: 3.53σ and 3.47σ for the filled and hollow model, respectively.

We continued our verification of the quality of the filled and hollow raspberry model, by examining hydrodynamic coupling between spheres rotating in unison in the same geometry as before, see Fig. 3(c). Figure 7 shows a comparison of our results to the expression given by Hofman *et al.* [4] for the box-size dependence of the rotational diffusion coefficient D_L^R . The procedure used to generate this data is analogous to that outlined for the translational experiments. Again, using the Stokes-Einstein equation

$$D_0^R = \frac{k_B T}{8\pi\eta (R_h^T)^3} \quad (23)$$

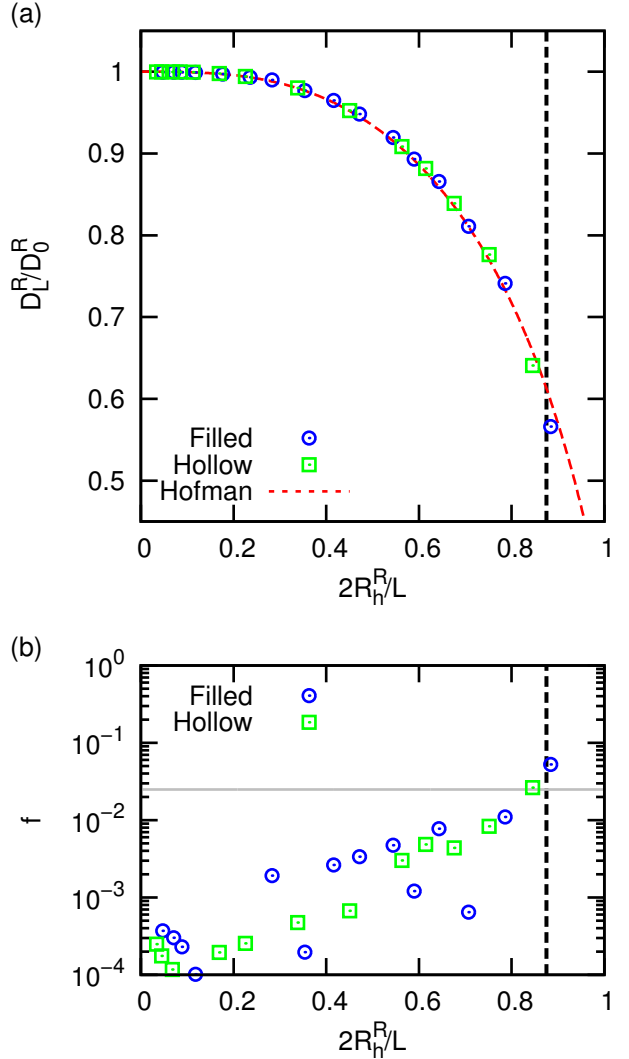


FIG. 7. (color online) (a) The dependence of the particle’s rotational diffusion coefficient D_L^R (expressed in terms of the bulk rotational diffusion coefficient D_0^R) on the inverse box length times the hydrodynamic diameter (twice the hydrodynamic radius R_h^R). The blue circles show results obtained for the filled raspberry and the green squares for the hollow raspberry. The red dashed curve shows the expression given by Hofman *et al.* [4] The vertical dashed black line indicates the value of L , for which the spheres are separated by one lattice spacing. (b) Fractional deviation f as a function of $2R_h^R/L$. The blue circles and green squares indicate the difference between the filled and hollow raspberry and analytic expression, respectively. The gray horizontal line indicates a fractional deviation of 2.5%.

we determined the effective hydrodynamic radius R_h^R from our data. Note that while there is still a systematic signature in f , see Fig. 7(c), the agreement between our result and literature is excellent for both models.

This further demonstrates the plausibility of our assessment that the high level of deviation for the transla-

tional diffusion is caused by the back-force/velocity that is applied homogeneously to the fluid, since a similar correction is not required for the rotational experiments. However, there is a fundamental difference between the experiments. The rotational motion exposes the fluid to constantly varying coupling points (the MD beads), whereas for translational motion the fluid could more easily find a pathway of least resistance. Again we observed that the effective hydrodynamic radii obtained for the hollow and filled raspberry differ significantly, 3.38σ and 3.54σ , respectively. It should be stressed that the fact that behavior of D_L^R is the same for both models, does not imply hydrodynamic consistency of the model, when we compare the value of R_h^T and R_h^R for the same model, which we will do next.

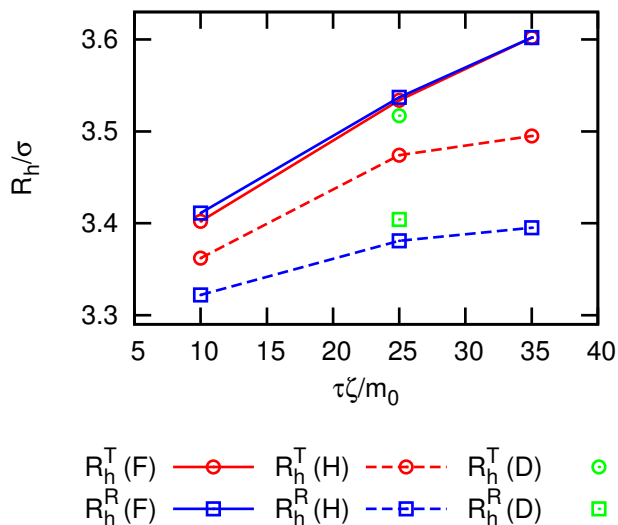


FIG. 8. (color online) The bulk effective hydrodynamic radii (translational R_h^T , rotational R_h^R) for the filled (F), hollow (H), and dense (D) raspberry models, respectively, as a function of the friction coefficient expressed in LB units (time τ and mass m_0).

To further assess the significance of the difference in effective hydrodynamic radius, we repeated our experiments for two other values of the bare friction ζ_0 . The results for the box-size dependence were in quantitative agreement. Our results for the hydrodynamic radii are summarized in Fig. 8. These effective hydrodynamic radii were obtained by extrapolation to the bulk value of the diffusion coefficient and utilizing the Stokes-Einstein relation. Note that the translational and rotational radii of the hollow raspberry differ substantially. This result is in agreement with the findings of Ollila *et al.* [18] The mismatch occurs for all values of the friction coefficient examined.

We also performed experiments with a hollow raspberry that had the same number of surface beads as the total number of beads used in the filled raspberry

– we refer to this model as the dense raspberry. This allowed us to examine the possibility of an increased effective friction with greater bead numbers, leading to a better match between rotational and translational hydrodynamic radius. [18] A similar discrepancy between R_h^T and R_h^R was found for the dense model, see Fig. 8. In fact, the deviation is slightly increased, which can be attributed to a slightly better fluid coupling at the surface. Our result for the dense raspberry indicates that the observed mismatch is not related to the number of beads used, only to their spatial distribution.

Finally, we examined the fluid-particle coupling to determine the cause of the inconsistency between the effective hydrodynamic radii that were obtained using the hollow raspberry model. Figure 9(a) shows the flow field around a hollow and filled spherical raspberry, rotating at constant angular velocity about the axis pointing into the page. From the flow field it becomes apparent that the coupling of the raspberry to the fluid has more lattice artifacts for the hollow raspberry than for the filled one (is less smooth). We quantified this difference further by examining the fluid velocity inside the particle, see Fig. 9(b). While the filled raspberry shows a linear increase in the velocity with the distance from the center (similar to the so-called ‘Rankine vortex state’), the hollow raspberry shows a clear kink in the velocity profile. This kink can be attributed to the diminished fluid-particle coupling away from the shell of MD beads.

B. Dumbbell in a Simple Cubic Crystal

Thus far, we have concentrated on the quality of the raspberry approximation for convex objects, namely the specific case of a spherical particle. In order to assess the raspberry model’s ability to capture the hydrodynamic properties of a non-convex particle, we considered two dumbbell-shaped raspberries, as shown in Fig. 2. We took care to create a raspberry model for which the two spheres touch, when the effective hydrodynamic radius of the MD beads is taken into account, also see Fig. 2 (left). Also note that for a dumbbell-shaped particle the grand hydrodynamic diffusion tensor (GHDT) has a diagonal form, with translational diffusion coefficients in the top-left 3×3 block (sub-matrix) and rotational ones in the lower-right 3×3 block. There are no cross-coupling terms due to symmetry considerations. [41, 42] In this section, we only show results for filled raspberries.

Our results for the dumbbell particles are qualitatively similar to the ones shown for the spherical colloid discussed above. Namely, we found the box-size dependence to be of the form $D_{L,i}^X = D_{0,i}^X (1 + a_i/L + b_i/L^3)$, with X either R or T and i either \perp or \parallel , and a_i and b_i coefficients. However, we could not compare our results to analytic calculations, since, to the best of our knowledge, such expressions have not been formulated. We therefore considered the extrapolated bulk diffusion coefficients only. Using both quiescent and thermalized sim-

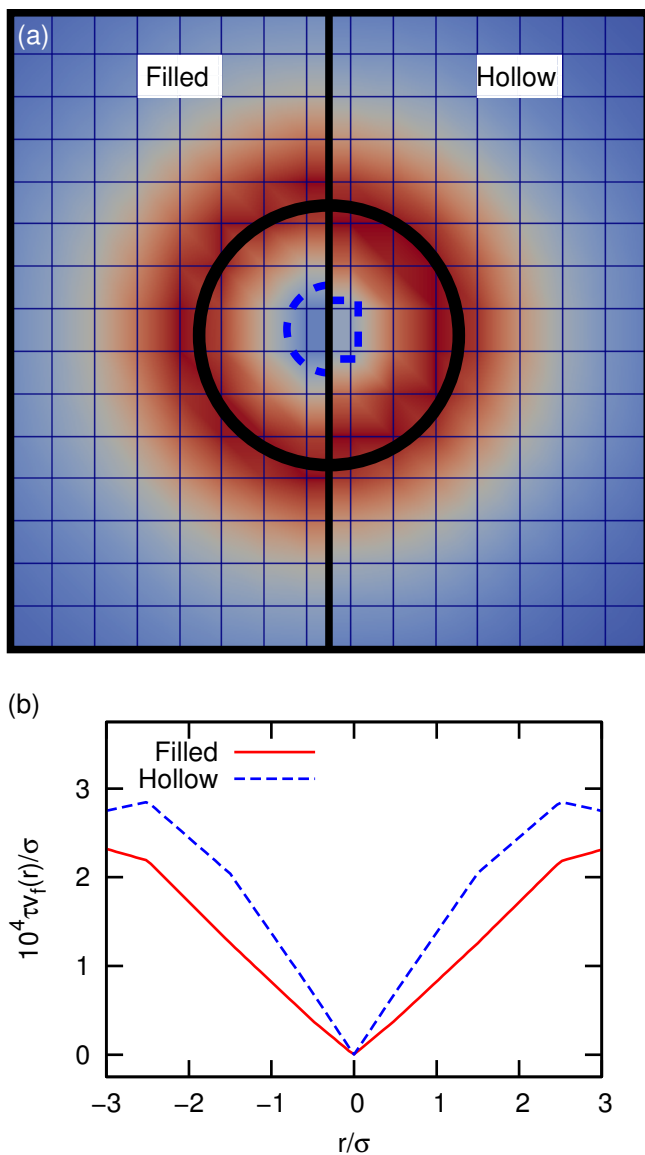


FIG. 9. (color online) Comparison of the flow field around a filled and hollow raspberry, respectively, undergoing a constant rotation. (a) Two dimensional plane through the center of the sphere with a normal that is parallel to the axis of rotation. The result for the filled raspberry is shown on the left and for the hollow variant on the right. The color coding gives the magnitude of the fluid velocity on the grid (blue lines). The thick black circle roughly indicates the position of the coupling points (at $|\mathbf{r}| = R$). The dashed blue semi circle and half square serve as guides to the eye for the structure of the flow field inside the raspberry. (b) Magnitude of the fluid velocity $v_f(r)$ – expressed in MD units of time, τ , and position σ – as a function of position r along the black vertical divide in (a). Only the value inside of the raspberry is shown for the filled (red, solid) and hollow (blue, dashed) particle.

ulations we verified that the GHDT had the expected form, all off-diagonal coefficients were orders of magnitude smaller than the on-diagonal elements and zero

Method	D_{\parallel}^T/D_0^T	D_{\perp}^T/D_0^T	D_{\parallel}^R/D_0^R	D_{\perp}^R/D_0^R
$d = 7\sigma / d = 2.00 \mu\text{m}$				
Raspberry	0.77 ± 0.01	0.69 ± 0.01	0.55 ± 0.01	0.27 ± 0.01
Hydro++	0.79 ± 0.01	0.69 ± 0.01	0.57 ± 0.01	0.27 ± 0.01
$d = 5\sigma / d = 1.43 \mu\text{m}$				
Raspberry	0.82 ± 0.01	0.74 ± 0.01	0.59 ± 0.01	0.36 ± 0.01
Hydro++	0.84 ± 0.01	0.75 ± 0.01	0.64 ± 0.01	0.37 ± 0.01

TABLE I. Comparison between the results obtained using the raspberry model and *HYDRO++* [44] for the translational (T) and rotational (R) diffusion coefficients in the direction parallel (\parallel) and perpendicular (\perp) to the main axis of a dumbbell in bulk fluid. The diffusion coefficients are normalized by the bulk values for a sphere with the same radius as one of the spheres comprising the dumbbell.

within the error bars. Moreover, we found that for both the translational and rotational diffusion sub-matrices, the two entries corresponding to perpendicular motion were equal (within the error) and the parallel component was larger, as expected. Table I lists these diffusion coefficients. In order to de-dimensionalize the results, we divided the diffusion coefficients by the translational and rotational diffusion coefficient of a sphere with radius $R = 3\sigma$, respectively.

To validate our model for the simulation of anisotropic non-convex particles, we compared our data with the results obtained using the *HYDRO++* program. [43, 44] *HYDRO++* is a tool used to evaluate the hydrodynamic properties of macromolecules and has been successfully utilized in comparisons to experimental data for anisotropic colloids consisting of (penetrating) spheres. [45] We determined the GHDT using *HYDRO++* for dumbbells consisting of two beads with radii $R = 1.0 \mu\text{m}$ at positions $(\pm 1.0, 0, 0) \mu\text{m}$ and $(\pm 0.714, 0, 0) \mu\text{m}$, respectively, in a fluid of viscosity $10^{-3} \text{ kg m}^{-1} \text{ s}^{-1}$ and density 10^3 kg m^{-3} with temperature $T = 293.15 \text{ K}$. We assumed that the particle has the same density as the fluid. The numerical algorithm is parametrized as follows: $H = 26$, $H_{\text{max}} = 1.5 \cdot 10^7$, $R_{\text{max}} = 80.0 \cdot 10^{-8}$, and $N_{\text{TRIALS}} = 10,000$; which are *HYDRO++* internal commands. The number of intervals for the distance distribution was set to 30.

The results of this comparison are summarized in Table I, in which we specify the diffusion coefficients for the filled raspberry and the ones determined using *HYDRO++*. The agreement for the bulk diffusion coefficients is quite excellent. This leads us to believe that the raspberry model may be applied to more complex (non-convex) geometries, without giving rise to significant errors.

IV. DISCUSSION

In Section III we have demonstrated that there is excellent agreement between established theoretical and nu-

merical results for the hydrodynamic behavior of convex and non-convex particles with their raspberry equivalent. In addition, we have shown that filling the raspberry model significantly improves the agreement between the effective hydrodynamic radius obtained by translational and rotational experiments. In this section we discuss this discrepancy between the effective hydrodynamic radii in more detail.

The inconsistency between the translational and rotational diffusion coefficient was first pointed out by Ollila *et al.* [18] However, the solution to remedy the discrepancy between the two results presented by Ollila *et al.* is more complicated than ours. They removed the stochastic term in the point-wise coupling force of one particle. In agreement with the observations of Ahlrichs and Dünweg, [13] Ollila *et al.* noticed that the kinetic temperature of the particle, measured *via* the equipartition theorem, and the temperature of the fluid differ significantly. By carefully tailoring the fluid-particle coupling, they succeeded in matching the rotational and translational effective radii, as well as the kinetic and fluid temperature. However, the agreement that we obtain for the filled raspberry demonstrates that such complicated procedures are unnecessary and can be avoided by simply adding MD beads to the interior.

A closer examination of the data presented in the original raspberry paper by Lobaskin and Dünweg [14] shows that the trends observed in our work are captured by their data points. Lobaskin and Dünweg erroneously assumed that the radius of the particle was the same as the radius R at which they positioned their MD beads. However, within the numerical uncertainty present in their results and the computational abilities of the time, this extrapolation to bulk was completely justifiable. By re-examining the data points of Ref. [14], we conclude that it is possible to fit the following bulk diffusion coefficients

$$D_0^T = (0.97 \pm 0.02) \frac{k_B T}{6\pi\eta R}; \quad (24)$$

$$D_0^R = (0.90 \pm 0.02) \frac{k_B T}{8\pi\eta R^3}. \quad (25)$$

This indicates that there is indeed an effective radius, $R_h^T = (1.03 \pm 0.02)R$ and $R_h^R = (1.03 \pm 0.01)R$, but the data is not of sufficient quality to assess whether there is a difference between the effective translational and rotational hydrodynamic radius.

Chatterji and Horbach [17] carried out a more thorough examination of the effective translational hydrodynamic radius. However, they did not provide results for the rotational hydrodynamic radius, they only comment on having carried out such experiments. Our results in Fig. 8 for the value of R_h^T for the hollow raspberry are in quantitative agreement with Ref. [17]. We therefore deem it likely that a similar discrepancy would be present in the data of Ref. [17], especially considering the observation of Ref. [18].

Finally, Poblete *et al.* [23] did not report a difference in the bulk hydrodynamic radii using their MPCD method

for a hollow raspberry. They instead found agreement between the two. However, it is unclear how accurately Poblete *et al.* could extrapolate their results to the bulk value, as in MPCD one always works with thermalized and therefore noisy data. Moreover, it is not obvious how large the effect ($R_h^T \neq R_h^R$) would be for their high-speed-of-sound systems.

The fractional difference in hydrodynamic radii of approximately $0.1\sigma/3.4\sigma = 0.03$ for the hollow raspberry may seem perfectly acceptable for most applications. However, one should be careful, since this small fraction can lead to a 10% discrepancy between the expected translational and rotational diffusion coefficient; had we assumed the effective hydrodynamic radius for rotational motion to be the same as that for translational motion. For processes where both translational and rotational diffusion play an important role, this could lead to significant deviation from the expected behavior. Moreover, we have shown that this is a general property of the raspberry colloid that does not resolve itself by increasing the particle-fluid coupling, see Fig. 9; as was also pointed out in Ref. [18]. Fortunately, by filling the raspberry, this problem can be overcome.

With regards to the filling procedure, we obtained a consistent result for translational and rotational diffusion for the number of MD beads we added to the interior of the particle. However, it is quite likely that similar results may be achieved by adding far fewer particles to the interior of the model, which will improve the computational performance of a simulation. Finally, it is worth noting that by increasing the radius of the raspberry, the problem may be substantially reduced as well, as the difference between the effective radii becomes less important for larger R . The need for filling, increasing R , or both should be examined on a per-simulation-study basis.

V. CONCLUSION AND OUTLOOK

Summarizing, we have examined the properties of the raspberry model using a variety of classic fluid dynamics experiments that predominantly focused on the long-time diffusion properties of these particles. This so-called ‘raspberry’ model refers to a hybrid lattice-Boltzmann (LB) and Langevin molecular dynamics (MD) scheme for simulating the dynamics of suspensions of colloids originally developed by Lobaskin and Dünweg. [14] The particle is represented by a set of points on its surface that couple to the fluid through a frictional force acting both on the solvent and on the solute, which depends on the relative velocity. We considered the hydrodynamic properties of spherical raspberries, as well as dumbbell-shaped raspberry particles in the low Reynold’s number limit. Our results show that the proper behavior in this limit is reproduced to a surprising degree of accuracy over a wide range of length scales for both convex and non-convex particle shapes.

From our combined data we can draw the follow-

ing conclusions concerning the quality of the raspberry model.

- Using a raspberry model to approximate a particle’s coupling to an LB fluid gives rise to an effective hydrodynamic radius. This effective radius must be properly taken into account in matching to the (experimental) system of interest. Our result is in agreement with the findings of Chatterji and Horbach. [17]
- The traditional ‘hollow’ raspberry model – an empty shell of MD coupling beads that describes the particle’s surface – gives rise to a discrepancy between the translational and rotational effective hydrodynamic radius. This effect was first pointed out by Ollila *et al.* [18]
- We find that the aforementioned mismatch can be easily and fully remedied by ‘filling’ the raspberry. That is, including MD coupling points with the fluid in the interior of the hollow shell.
- The raspberry model can be used on both convex and non-convex particles. We verified this for the specific case of a dumbbell-shaped particle, but our results may be safely extrapolated to more complicated shapes. However, the effective hydrodynamic radius of the raspberry must be properly taken into account. That is, the MD beads must be positioned in such a way that the effective hydrodynamic hull, which forms around these points, approximates the shape of the particle of interest.
- The force and velocity experiments traditionally performed to determine the translational diffusion coefficient in a cubic geometry with periodic boundary conditions are problematic for small boxes compared to the particle size. The back force/velocity density that must be applied to the fluid to maintain zero center of mass velocity, leads to difficulties in interpretation the mobility data that is obtained from these experiments. We find that the net/effective force acting on the particle is given by the applied force minus the back force density

integrated over the volume that the raspberry occupies. Utilizing this net force gives a better match with numerical results for the solution to Stokes’ equations in this geometry. [4, 8, 9] A similar result follows for the velocity experiment. The application of a back force/velocity density is also a candidate for the observed disagreement between the thermal and quiescent data at intermediate and long time scales.

From the above, it becomes clear that the raspberry model is an excellent way to approximate fluid-particle coupling in an LB algorithm. We have expanded upon previous studies that verified the model’s properties, see, for example Refs. [14, 17, 18]. However, there remain several open problems to be addressed in future studies. We have shown that the short-time behavior of the raspberry model (for the LB parameters used in this manuscript) is quite different from the low Reynold’s number solution to the Navier-Stokes equations. This raises the question of how accurately the short-time regime of colloid dynamics can be captured using the raspberry model. An accurate description of such short-time processes would be relevant for, e.g., nucleation and crystallization. [46] A possible solution is to change from a Langevin dynamics to an overdamped (Brownian) dynamics description for the fluid particle coupling.

All in all, the original as well as our improved raspberry model have proven themselves to be very powerful means to approximate translational as well as rotational fluid-particle coupling.

ACKNOWLEDGEMENTS

J.d.G. acknowledges financial support by a “Nederlandse Organisatie voor Wetenschappelijk Onderzoek” (NWO) Rubicon Grant (#680501210). We thank the “Deutsche Forschungsgemeinschaft” (DFG) for financial funding through the SPP 1726 “Microswimmers – from single particle motion to collective behavior”. We are also grateful to O. Hickey and S. Kesselheim for useful discussions.

-
- [1] L. Euler, Mem. Acad. Sci. Inst. Berlin **11**, 274 (1757).
 - [2] C. Navier, Mem. Acad. Sci. Inst. France **6**, 389 (1822).
 - [3] G. Stokes, Trans. Cambridge Phil. Soc. **8**, 287 (1849).
 - [4] J. Hofman, H. Clercx, and P. Schram, Physica **268**, 353 (1999).
 - [5] J. Giddings, Separ. Sci. Technol. **13**, 241 (1978).
 - [6] R. Noel, K. Gooding, F. Regnier, C. Orr, and M. Mullins, J. Chromatogr. A **166**, 373 (1978).
 - [7] J. de Graaf, T. Peter, L. Fischer, and C. Holm, J. Chem. Phys. **submitted**, (2015).
 - [8] H. Hasimoto, J. Fluid Mech. **5**, 317328 (1959).
 - [9] A. Zick and G. Homsy, J. Fluid Mech. **115**, 13 (1982).
 - [10] H. Brenner, J. Colloid and Interface Sci. **32**, 141 (1970).
 - [11] M. Zuzovsky, P. Adler, and H. Brenner, Phys. Fluids **26**, 1714 (1983).
 - [12] B. Dünweg and A. Ladd, Lattice boltzmann simulations of soft matter systems, in Advanced Computer Simulation Approaches for Soft Matter Sciences III, edited by C. Holm and K. Kremer, volume 221 of Adv. Polymer Sci., pages 89–166, Springer (Berlin/Heidelberg), 2009.
 - [13] P. Ahrlichs and B. Dünweg, J. Chem. Phys. **111**, 8225 (1999).
 - [14] V. Lobaskin and B. Dünweg, New J. Phys. **6**, 54 (2004).

- [15] A. Ladd, *J. Fluid Mech.* **271**, 285 (1994).
- [16] C. Aidun and Y. Lu, *J. Stat. Phys.* **81**, 49 (1995).
- [17] A. Chatterji and J. Horbach, *J. Chem. Phys.* **122**, 184903 (2005).
- [18] S. Ollila, C. Smith, T. Ala-Nissila, and C. Denniston, *Multiscale Model. Simul.* **11**, 213 (2013).
- [19] V. Lobaskin, B. Dünweg, M. Medebach, T. Palberg, and C. Holm, *Phys. Rev. Lett.* **98**, 176105 (2007).
- [20] V. Lobaskin, D. Lobaskin, and I. Kulić, *Eur. Phys. J. Spec. Top.* **157**, 149 (2008).
- [21] S. Raafatnia, O. Hickey, and C. Holm, *Phys. Rev. Lett.* **113**, 238301 (2014).
- [22] M. Belushkin, R. Winkler, and G. Foffi, *J. Phys. Chem. B* **115**, 14263 (2011).
- [23] S. Poblete, A. Wysocki, G. Gompper, and R. Winkler, *Phys. Rev. E* **90**, 033314 (2014).
- [24] J. Sané, J. Padding, and A. Louis, *Phys. Rev. E* **79**, 051402 (2009).
- [25] F. Lugli, E. Brini, and F. Zerbetto, *J. Phys. Chem. C* **116**, 592 (2012).
- [26] J. Zhou and F. Schmid, *Eur. Phys. J. E* **36** (2013).
- [27] H. J. Limbach, A. Arnold, B. A. Mann, and C. Holm, *Comp. Phys. Comm.* **174**, 704 (2006).
- [28] A. Arnold et al., ESPResSo 3.1 — Molecular Dynamics Software for Coarse-Grained Models, in *Meshfree Methods for Partial Differential Equations VI*, edited by M. Griebel and M. A. Schweitzer, volume 89 of *Lecture Notes in Computational Science and Engineering*, page 1, Springer, 2013.
- [29] D. Roehm and A. Arnold, *Eur. Phys. J. ST* **210**, 73 (2012).
- [30] D. d’Humières, I. Ginzburg, M. Krafczyk, P. Lallemand, and L.-S. Luo, *Philos. Trans. A Math. Phys. Eng. Sci.* **360**, 437 (2002).
- [31] R. Adhikari, K. Stratford, M. E. Cates, and A. J. Wagner, *Euro. Phys. Lett.* **71**, 473 (2005).
- [32] B. Dünweg, U. Schiller, and A. Ladd, *Phys. Rev. E* **76**, 036704 (2007).
- [33] B. Dünweg, U. Schiller, and A. Ladd, *Comp. Phys. Commun.* **180**, 605 (2009).
- [34] J. Padding and A. Louis, *Phys. Rev. E* **74**, 031402 (2006).
- [35] A. Louis, *Faraday Discuss.* **144**, 323 (2010).
- [36] J. Ramirez, S. Sukumaran, B. Vorselaars, and A. Likhtman., *J. Chem. Phys.* **133**, 154103 (2010).
- [37] J.-P. Hansen and I. McDonald, *Theory of Simple Liquids*, Academic Press (London), 2nd edition, 1986.
- [38] M. Friese, T. Nieminen, N. Heckenberg, and H. Rubinsztein-Dunlop, *Nature* **394**, 348 (1998).
- [39] B. Grzybowski, H. Stone, and G. Whitesides, *Nature* **405**, 1033 (2000).
- [40] B. Grzybowski, X. Jiang, H. Stone, and G. Whitesides, *Phys. Rev. E* **64**, 011603 (2001).
- [41] H. Brenner, *J. Colloid Sci.* **20**, 104 (1965).
- [42] H. Brenner, *J. Colloid Interface Sci.* **23**, 407 (1967).
- [43] J. G. de la Torre and V. Bloomfield, *Q. Rev. Biophys.* **14**, 81 (1981).
- [44] J. G. de la Torre, G. del Rio, and A. Ortega, *J. Phys. Chem. B* **111**, 955 (2007).
- [45] D. Kraft et al., *Phys. Rev. E* **88**, 050301 (2013).
- [46] D. Roehm, S. Kesselheim, and A. Arnold, *Soft Matter* **10**, 5503 (2014).